Supporting Information

In situ characterization of cofacial Co(IV) centers in Co_4O_4 cubane: Modeling the high-valent active site in oxygen evolving catalysts

Casey N. Brodsky,[a,1] Ryan G. Hadt,[b,1] Dugan Hayes,[b] Benjamin J. Reinhart,[b] Nancy Li,[a] Lin X. Chen[b,c] and Daniel G. Nocera[a]

[a] *Department of Chemistry and Chemical Biology, 12 Oxford Street, Harvard University, Cambridge, Massachusetts 02138*

[b] *Chemical Sciences and Engineering Division, 9700 S. Cass Avenue, Argonne National Laboratory, Lemont, Illinois 60439*

[c] *Department of Chemistry, 2145 Sheridan Road, Northwestern University, Evanston, Illinois 60208.*

Email: dnocera@fas.harvard.edu

Table of Contents *Page*

A. Experimental Methods

A.1. Synthesis

Synthesis of neutral Co_4O_4 cubane, $Co_4O_4(OAc)_4(py)_4$ (**1**), was performed as described in a previous publication (*1*). Crude $Co_4O_4(OAc)_4(py)_4$ was prepared according to the procedures of Dismukes (*2*) and Bonchio (*3*). Purification of **1** was performed on a Biotage Isolera One automated flash chromatography system using a mobile phase gradient of 2–10% methanol/dichloromethane. A typical loading ratio was 10 mg of crude material for 1 g of silica. Samples were loaded onto the columns using a minimal volume of dichloromethane. Typical yields after purification were 40–50%. Spectra of **1** (^{1}H NMR and mass spectrometry) were consistent with those reported in the literature (*1*).

A.2. Electrochemistry

Cyclic voltammograms (CVs) were recorded using a CH Instruments potentiostat. **1** was dissolved to a 1 mM concentration in a solution containing a supporting electrolyte, 0.1 M *n*-Bu_4NPF_6 (purchased from Sigma Aldrich, used without any purification and stored under vacuum) in acetonitrile (previously purified and dried by passing through a neutral alumina column under argon). CV experiments were conducted in a glovebox under an atmosphere of nitrogen, using a CH instruments glassy carbon working electrode (area = 0.076 cm^2), a Pt wire counter electrode, and an Ag wire in 0.1 M M *n*-Bu_4NPF_6/MeCN as a reference electrode. The glassy carbon working electrode was carefully polished before each measurement. The polishing procedure was performed for 2 min on felt using different diamond pastes subsequently of 15, 6, 3 and 1 μm. Ethanol was used as a lubricant and to remove the diamond paste from the electrode. Before use, electrodes were briefly sonicated in ethanol and dried with a stream of compressed air. The ohmic drop was carefully compensated in all electrochemical experiments by using the positive feedback compensation. After each CV experiment, potentials were referenced using ferrocene as an internal standard.

Thin-layer UV-Vis spectroelectrochemistry experiments were performed using a 0.05 cm path length quartz cell with an Ocean Optics USB4000 spectrophotometer and DT-Mini-2GS UV-vis-NIR light source in conjunction with the CH electrochemical workstation described above. Samples were prepared as 2 mM of compound **1** in 0.1 M *n*-Bu_4NPF_6 in MeCN. Bulk electrolysis was performed using a Pt flag working electrode, an Ag wire refer-

1. Ullman AM, Liu Y, Huynh M; Bediako DK, Wang H, Anderson BL, Powers DC, Breen JJ, Abruna HD, Nocera DG (2014) Water oxidation catalysis by Co(II) impurities in $Co(III)_4O_4$ cubanes. *J Am Chem Soc* 136:17681–17688.
2. McCool NS, Robinson DM, Sheats JE, Dismukes GC (2011) A Co_4O_4 "cubane" water oxidation catalyst inspired by photosynthesis. *J Am Chem Soc* 133:11446–11449.
3. Berardi S, L Ganga G, Natali M, Bazzan I, Puntoriero F, Sartorel A, Scandola F, Campagna S, Bonchio M (2012) Photocatalytic water oxidation: tuning light-induced electron transfer by molecular Co_4O_4 cores. *J Am Chem Soc* 134:11104–11107.

ence electrode, and a Pt wire counter electrode. Near-IR spectroelectrochemical experiments were performed with the same cell and electrodes, but with a 16.7 mM solution of **1** in *n*-Bu_4NPF_6 in deuterated MeCN, and spectra were acquired with an Agilent Cary 60 UV-vis-nIR spectrophotometer.

A.3. X-ray Spectroscopic Methods

Co K-edge (~7709 eV) XANES data were collected at beamline 12-BM-B at the Advanced Photon Source of Argonne National Laboratory using a water-cooled, double-crystal, fixed-exit monochromator with Si(111) crystals and a double mirror system (flat plus toroidal) with a cutoff energy of 23 keV to focus the beam to ~0.5 mm (v) × 1 mm (h). All data were collected in fluorescence mode using a liquid nitrogen cooled Canberra 13-element Ge detector. All data are referenced to Co foil. Data were collected at room temperature in a home-built spectroelectrochemical X-ray spectroscopic cell. The cell design will be published elsewhere; its construction closely matched the dimensions of the quartz optical spectroelectrochemical cell. This allowed for an identical three-electrode setup between optical and X-ray spectroelectrochemical cells. In order to avoid X-ray sample damage/reduction, data were collected on multiple sample positions. Two to three scans, each at different sample positions, were averaged for analysis. Background subtraction and data normalization were carried out using the Athena software package (*4*).

A.4. Computational Methods

All DFT calculations were carried out using Gaussian 09 (*5*), revision A.02, software installed on the Blues or Fusion clusters at Argonne National Laboratory. All orbital surfaces were generated using the β-LUMO program (*6*). Geometry optimizations were carried out using a modified BP86 functional (*7*–*9*) (spin unrestricted for paramagnetic states), in

4. Ravel B, Newville, M (2005) ATHENA, ARTEMIS, HEPHAESTUS: data analysis for x-ray absorption spectroscopy using IFEFFIT. *J Synch Rad* 12:537–541.
5. Frisch MJ, Trucks GW, Schlegel HB, Scuseria GE, Robb MA, Cheeseman JR, Scalmani G, Barone V, Mennucci B, Petersson GA, Nakatsuji H, Caricato M, Li X, Hratchian HP, Izmaylov AF, Bloino J, Zheng G, Sonnenberg JL, Hada M, Ehara M, Toyota K, Fukuda R, Hasegawa J, Ishida M, Nakajima T, Honda Y, Kitao O, Nakai H, Vreven T, Montgomery JA Jr, Peralta JE, Ogliaro F, Bearpark M, Heyd JJ, Brothers E, Kudin KN, Staroverov VN, Keith T, Kobayashi R, Normand J, Raghavachari K, Rendell A, Burant JC, Iyengar SS, Tomasi J, Cossi M, Rega N, Millam JM, Klene M, Knox JE, Cross JB, Bakken V, Adamo C, Jaramillo J, Gomperts R, Stratmann RE, Yazyev O, Austin AJ, Cammi R, Pomelli C, Ochterski JW, Martin RL, Morokuma K, Zakrzewski VG, Voth GA, Salvador P, Dannenberg JJ, Dapprich S, Daniels AD, Farkas O, Foresman JB, Ortiz JV, Cioslowski J, Fox DJ (2009) *Gaussian 09*, revision A.01; Gaussian, Inc.: Wallingford, CT.
6. Kieber-Emmons MT (2009) β-LUMO, Version 0.9b; Burlingame, CA.
7. Perdew JP (1986) Density-functional approximation for the correlation energy of inhomogeneous electron gas. *Phys Rev B* 33:8822–8824.
8. Becke AD (1988) Density-functional exchange-energy approximation with correct asymptotic behavior. *Phys Rev A* 38:3098–3100.
9. Becke AD (1993) Density-functional thermochemistry. III. The role of exact exchange. *J Chem Phys* 98:5648–5652.

combination with a 6-311G(d) (*10–12*) basis set on all atoms. B(XXHF)P86 functionals were utilized wherein the amount of Hartree-Fock exchange could be varied from 15 – 25 %. The neutral geometry and symmetric structures (electronically delocalized) were geometry optimized using the B(15HF)P86 functional while asymmetrically distorted structures (electronically localized) were geometry optimized using the B(25HF)P86 functional. Stability checks were carried out to ensure wavefunctions represented minima. Single point calculations were carried out using the B(15HF)P86 functional, but with a split basis set (6-311+G(d) for Co, O, and N atoms, and 6-31G(d) for C and H atoms). We have previously shown *(13)* that at least 15% HF exchange is needed to give a partially localized ground state and to reproduce experimental reduction potentials for Co(IV) formation. We have therefore used the same methodology here for consistency. In some cases, the self-consistent field (SCF) convergence criteria were loosened (Energy: 1.0×10^{-4}, max density matrix: 1.0×10^{-4}, and RMS density matrix: 1.0×10^{-6}; units: Hartree). Solvation (acetonitrile) was included using the polarized continuum model (PCM) (*14*). The exchange coupling constant J was determined via Broken-Symmetry calculations using the following equation *(15,16)*, where ${}^{3}E$ is the energy of the triplet state, ${}^{BS}E$ is the energy of the BS state, and $\langle S^2 \rangle_{BS}$ is the expectation value of S^2 for the BS state:

$$-2J = {}^{3}E - \frac{2^{BS}E - \langle S^2 \rangle_{BS}\ {}^{3}E}{2 - \langle S^2 \rangle_{BS}} \qquad \text{(S1)}$$

We note that increasing the amount of HF exchange for single point calculation of J is analogous to decreasing the Mott-Hubbard U value in equation 5 of the main text, which should result in J values that are less negative. For example, increasing the amount of HF exchange to 20% (B3LYP) results in J values of –130 and –16 cm^{-1} for *cis*-Py and *cis*-OAc, respectively.

10. Francl MM, Pietero WJ, Hehre WJ, Binkley JS, Gordon MS, DeFrees DJ, Pople JA (1982) Self-consistent molecular orbital methods. XXIII. A polarization-type basis set for second-row elements. *J Chem Phys* 77:3654–3665.
11. Hariharan PC, Pople JA (1973) Influence of polarization functions on MO hydrogenation energies. *Theor Chim Acta* 28:213–222.
12. Rassolov VA, Pople JA, Ratner MA, Windus TL (1998) 6-31G* basis set for atoms K through Zn *J Chem Phys* 109:1223–1229.
13. Hadt RG, Hayes D, Brodsky CN, Ullman AM, Casa DM, Upton MH, Nocera DG, Chen LX (2016) X-ray spectroscopic characterization of Co(IV) and metal-metal interactions in Co4O4: electronic structure contributions to the formation of high-valent states relevant to the oxygen evolution reaction. *J Am Chem Soc* 138:11017–11030.
14. Miertus S, Scrocco E, Tomasi, J (1981) Electrostatic interaction of a solute with a continuum. A direct utilization of ab initio molecular potentials for the prevision of solvent effects. *Chem Phys* 55:117–129.
15. Noodleman, L (1981) Valence bond description of antiferromagnetic coupling in transition metal dimer. *J Chem Phys* 74:5737–5743.
16. Noodleman L, Case DA (1992) Density-functional theory of spin polarization and spin coupling in iron-sulfur clusters. *Adv Inorg Chem* 38:423–470.

B. Electron Transfer Calculations

B.1. Comproportionation Constant

A comproportionation constant for the equilibrium $Co(III)_4 + Co(III)_2(IV)_2 \rightarrow 2Co(III)_3(IV)$ is calculated from the CV of **1** (Figure 2 in main text) using Eq. S2 (*17*), where ΔE is the difference in potential between the first and second oxidation waves. K_C was determined to be 3.05×10^{19}.

$$K_C = \exp\left(\frac{F\Delta E}{RT}\right) \tag{S2}$$

B.2. Heterogeneous ET Parameters

Scan rate-dependent CV experiments were used to extract the heterogeneous electron transfer rate constant. The peak current, i_p, of a CV depends on scan rate, v, and diffusion coefficient, D, and is described by the relationship given in Eq. S3, where S is the electrode surface area and C^0 is the substrate concentration (*18*). The splitting between anodic and cathodic peaks in a slow quasi-reversible ET redox couple depends on the heterogeneous ET rate constant k_s as given by Eq. S4, where α is the transfer coefficient and is generally taken as 0.5 (*18*).

$$i_p = 0.446FSC^0\sqrt{D}\sqrt{\frac{Fv}{RT}} \tag{S3}$$

$$\Delta E = \frac{RT}{\alpha F}\ln\left(k_s\sqrt{\frac{RT}{\alpha F v D}}\right) - 0.78\frac{RT}{\alpha F} \tag{S4}$$

DigiElch CV simulation software (*19*) was used to fit a CV of **1** obtained at v = 0.1 V/s to obtain the diffusion coefficient, $D = 5 \times 10^{-6}$ cm^2/s. Using this diffusion coefficient, a 10 V/s CV was fit to obtain the rate constant k_s according to Eq. S4. This fitting yielded k_s = 0.110 and 0.050 cm/s for the first and second oxidation waves, respectively. The ET rate constant is related to the total reorganization energy λ, comprising inner (λ_i) and outer sphere (λ_o) components as described by Eqs. S5 and S6, assuming that the pre-exponential factor is

17. D'Alessandro DM, Keene, FR (2004) A cautionary warning on the use of electrochemical measurements to calculate comproportionation constants for mixed-valence compounds. *Dalton Trans.* 3950–3954.
18. Savéant J-M (2006) *Elements of Molecular and Biomolecular Electrochemistry: An Electrochemical Approach to Electron Transfer Chemistry* (John Wiley, New Jersey), pp 28–62.
19. Rudolph M (2003) Digital simulations on unequally spaced grids: Part 2. Using the box method by discretisation on a transformed equally spaced grid. *J Electroanal Chem* 543:23–39.

equal to the collision frequency (*20*). Eqs. S4 and S5 were used to calculate λ for both cubane oxidations; λ = 1.00 and 1.08 eV were obtained for the first and second oxidations, respectively.

$$k_{\mathrm{s}} = z^{\mathrm{el}} \exp\left[\frac{-\Delta G_0^{\neq}}{\mathrm{RT}}\right] = z^{\mathrm{el}} \exp\left[\frac{-\lambda}{4\mathrm{RT}}\right] \tag{S5}$$

$$z^{\mathrm{el}} = \sqrt{\frac{\mathrm{RT}}{2\pi \mathrm{M}}} \tag{S6}$$

B.3. Intramolecular ET Parameters

Intramolecular ET parameters were extracted from IVCT bands of **1b** and **1c**. A theoretical bandwidth, $\Delta\nu_{1/2}^0$, is determined based on the energy of the IVCT, $\nu_{\max}$, (Eq. S7) and is compared to the experimental bandwidth to yield the ratio parameter Γ, (Eq. S8). Values of Γ between 0 and 0.5 classify species as Robin-Day Class II mixed valent. Γ was determined to be 0.24 and 0.07 for **1b** and **1c**, respectively (*21*–*23*).

$$\Delta\nu_{1/2}^0 = \sqrt{16\mathrm{RT}\ln(2)\nu_{\max}} \tag{S7}$$

$$\Gamma = 1 - \frac{\Delta\nu_{1/2}}{\Delta\nu_{1/2}^0} \tag{S8}$$

The electronic coupling factor H_{ab} is given by Eq. S9, and was determined to be 273 and 394 cm^{-1} for **1b** and **1c**, respectively, taking the value of $r_{\mathrm{ab}} = 2.786$ Å (*1*) as the average of the four Co-Co bonds in the crystal structure of **1**. The inner sphere reorganization energy associated with intramolecular ET, λ_{i}, is derived directly from $\nu_{\max}$ (Eq. S10) (*24*), yielding 0.67 and 0.74 eV, for **1b** and **1c**, respectively.

$$H_{\mathrm{ab}} = 0.0206\sqrt{\nu_{\max}\varepsilon_{\max}\Delta\nu_{1/2}}/r_{ab} \tag{S9}$$

20. Costentin C, Louault C, Robert M, Rogé V, Savéant J-M (2012) Reorganization energy and pre-exponential factor from temperature-dependent experiments in electron transfer reactions. A typical example: the reduction of tert-nitrobutane. *Phys Chem Chem Phys* 14:1581–1584.
21. Brunschwig BS, Creutz C, Sutin N (2002) Optical transitions of symmetrical mixed-valence systems in the Class II–III transition regime. *Chem Soc Rev* 31:168–184.
22. Chakraborty I, Baran P, Sanakis Y, Simopoulous A, Fachini E, Raptis RG (2008) A mixed-valence octanuclear iron–oxo pyrazolate: assessment of electronic delocalization by structural and spectroscopic analysis. *Inorg Chem* 47:11734–11737.
23. Gaudette AI, Jeon I-R, Anderson JS, Grandjean F, Long GJ, Harris TD (2015) Electron hopping through double-exchange coupling in a mixed-valence diiminobenzoquinone-bridged Fe_2 complex. *J Am Chem Soc* 137:12617–12626.
24. Kubiak CP (2013) Inorganic electron transfer: sharpening a fuzzy border in mixed valency and extending mixed valency across supramolecular systems. *Inorg Chem* 52:5663–5676.

$$\lambda_{\mathrm{i}} = \mathrm{hc}\nu_{\mathrm{max}} \tag{S10}$$

The thermal barrier to intramolecular ET, ΔG^*, and the associated intramolecular ET rate constant, k_{ET}, are derived from λ_{i} and H_{ab} as given in Eqs. S11 and S12, where κ and ν_{N} are taken as 1 and 5×10^{12}, respectively (*21,24,25*). ΔG^* = 1090 and 1130 cm^{-1} and $k_{\mathrm{ET}} = 3.22 \times 10^{12}$ and 3.17×10^{12} s^{-1} for **1b** and **1c**, respectively.

$$\Delta G^* = \frac{(\lambda_{\mathrm{i}} - 2H_{\mathrm{ab}})^2}{4\lambda_{\mathrm{i}}} \tag{S11}$$

$$k_{\mathrm{ET}} = \kappa \upsilon_N \exp\left[-\frac{\Delta G^*}{\mathrm{RT}}\right] \tag{S12}$$

25. Brunschwig BS, Sutin N (2001) Reflections on the two-state electron-transfer model in *Electron Transfer in Chemistry,* Vol 2. ed Balzani V (Wiley-VCH, New York), pp 583–615.

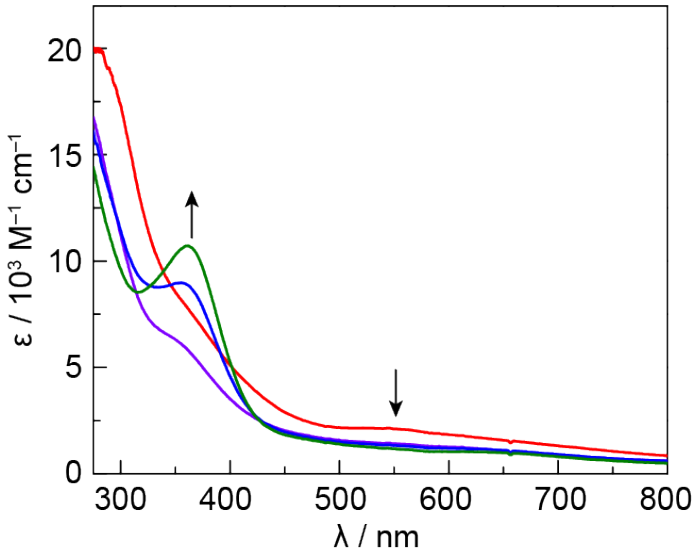

Fig. S1. Spectroelectrochemistry of **1**, performed in MeCN + 0.1 M *n*-Bu_4NPF_6. The cubane species in the spectral window was oxidized to the $Co(III)_2(IV)_2$ state by constant potential electrolysis (see Figure 2) and then the potential was removed and the system was allowed to sit at open circuit potential. UV-vis spectra were acquired at 0 (red —), 10 (purple —), 20 (blue —), and 30 (green —) min. After 30 min the spectrum had decayed to that of the neutral $Co(III)_4$ species, due to diffusion of oxidized species from the optical window.

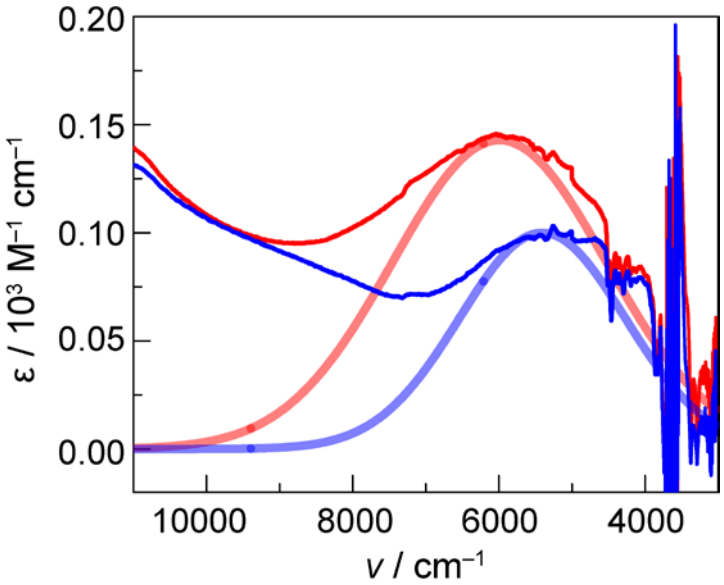

Fig. S2. Gaussian fits for the *in situ* IVCT data shown in Main Text Fig. 3, for **1b** (blue —) and **1c** (red —). Note that the Gaussian fits are partially complicated by the solvent background; however, the fits reported here represent lower limits on bandwidth and therefore upper limits on Γ.

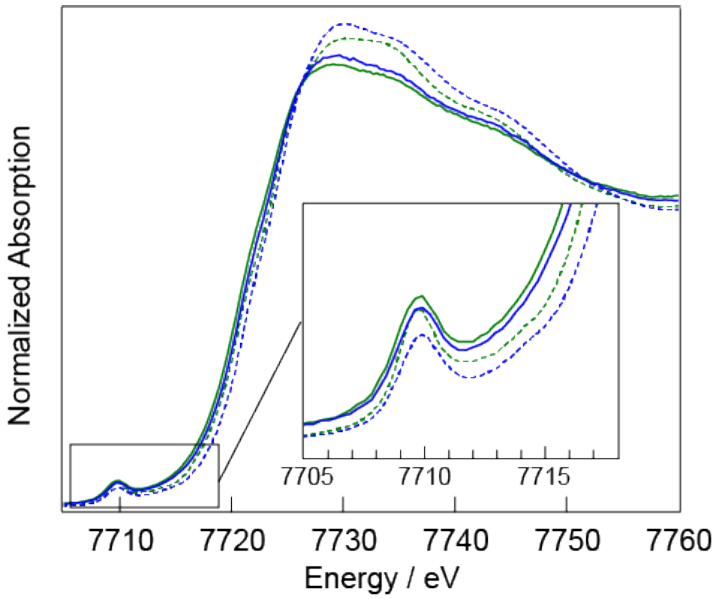

Fig. S3. X-ray spectroelectrochemistry of neutral **1a** and singly oxidized **1b** performed in MeCN + 0.1 M *n*-Bu_4NPF_6. Spectra were compared to X-ray absorption spectra of powder samples of both oxidation states: *in situ* neutral (green solid —), powder neutral (green dash — —), *in situ* oxidized (blue solid —), and powder oxidized (blue dash — —).

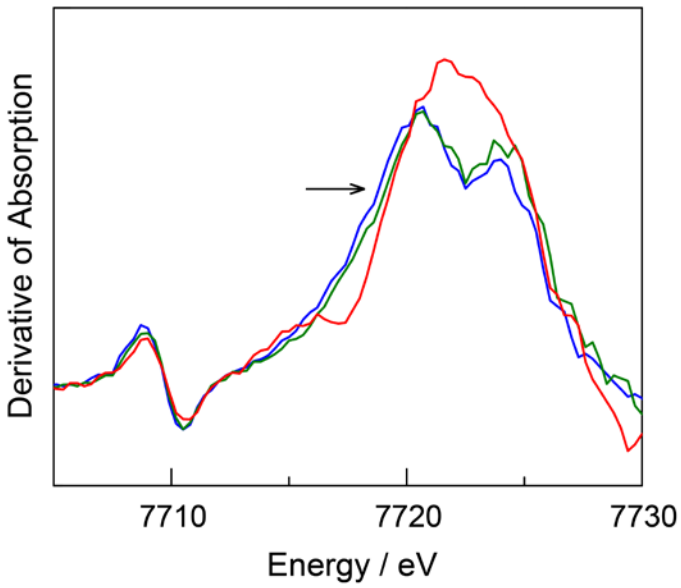

Fig. S4. First derivative of X-ray absorption spectra (given in Main Text Fig. 4) obtained by X-ray spectroelectrochemistry of the three accessible oxidation states of **1**, performed in MeCN + 0.1 M *n*-Bu_4NPF_6. Derivative spectra are shown for **1a** (green —), **1b** (blue —), and **1c** (red —), obtained by applying no potential, 0.80, and 1.8 V vs. $Fc^{+/0}$, respectively. Solutions of **1** are 2 mM. The cell path length is 0.1 cm.

Table S1. Mulliken spin densities and population analyses for the antiferromagnetic DFT solutions of **1c**.[a]

Cubane	Co	oxo	Py(N)	OAc(O)
1c (*cis*-py)	0.92/–0.92	0.05/–0.05	0.01/–0.01	0.05/–0.05
1c (*cis*-OAc)	0.78/–0.78	0.23/–0.23	0.02/–0.02	0.02/–0.02
1c (*cis*-py)[b]	75.1	13.3	6.3	0.7
1c (*cis*-py)[c]	75.1	13.4	6.3	0.7
1c (*cis*-OAc)[b]	68.5	16.5	11.0	0.2
1c (*cis*-OAc)[c]	68.2	17.2	10.4	0.2

[a] Total Mulliken spin densities and characters are given (Co, d; oxo, p; Py, N p; OAc, O p). [b] Mulliken population analysis of the α-LUMO, [c] Mulliken population analysis of the β-LUMO